



Quantum information preserving computational electromagnetics

Dong-Yeop Na , Jie Zhu, and Weng C. Chew *

School of Electrical and Computer Engineering, Purdue University, West Lafayette, Indiana 47906, USA

Fernando L. Teixeira

*ElectroScience Laboratory and Department of Electrical and Computer Engineering,
The Ohio State University, Columbus, Ohio 43212, USA*



(Received 24 August 2019; accepted 18 May 2020; published 13 July 2020)

We present a computational framework for canonical quantization in arbitrary inhomogeneous dielectric media by incorporating quantum electromagnetic effects into complex solutions of quantum Maxwell's equations. To do so, the proposed algorithm integrates and performs (1) numerical computation of normal modes and (2) evaluation of arbitrary products of ladder operators acting on multimode Fock states. The former is associated with Hermitian-Helmholtz linear systems using finite-element or finite-difference methods; consequently, the complete set of numerical normal modes diagonalizes the Hamiltonian operators up to floating-point precision. Its Hermiticity is retained, allowing its quantization. Then, we perform quantum numerical simulations of two-photon interference occurring in a 50:50 beam splitter to observe the Hong-Ou-Mandel effect. Our prototype model is useful for numerical analyses on various narrow-band quantum-optical multiphoton systems such as quantum metasurfaces, quantum-optical filters, and quantum electrodynamics in open optical cavities.

DOI: [10.1103/PhysRevA.102.013711](https://doi.org/10.1103/PhysRevA.102.013711)

I. INTRODUCTION

The recent advent of quantum computing spells the beginning of an exciting era for quantum technologies. Mathematical modeling of physical phenomena and their numerical simulations have transformed classical electromagnetics technologies. But this knowledge base is still in its infancy for quantum Maxwell's equations and quantum technologies. Quantum Maxwell's equations [1–5], where the classical Maxwell dynamic field and source variables are elevated to infinite-dimensional quantum *operators*, are

$$\begin{aligned}\nabla \times \hat{\mathbf{E}}(\mathbf{r}, t) &= -\frac{\partial \hat{\mathbf{B}}(\mathbf{r}, t)}{\partial t}, \\ \nabla \times \hat{\mathbf{H}}(\mathbf{r}, t) &= \hat{\mathbf{J}}(\mathbf{r}, t) + \frac{\partial \hat{\mathbf{D}}(\mathbf{r}, t)}{\partial t}, \\ \nabla \cdot \hat{\mathbf{D}}(\mathbf{r}, t) &= \hat{\rho}(\mathbf{r}, t), \\ \nabla \cdot \hat{\mathbf{B}}(\mathbf{r}, t) &= 0.\end{aligned}\quad (1)$$

The above quantum electromagnetics (QEM) equations are rigorously derived in the Heisenberg picture, in both coordinate and mode Hilbert spaces, in [1,2] and extended to inhomogeneous media with impressed sources. But the spatial and time (we shall call this coordinate) dependence of the field operators is similar to that of the classical Maxwell's equations.

The above quantum operator equations are meaningful only when they operate on a quantum state. The corresponding equation of motion for the quantum state is

$$\hat{H}|\psi(t)\rangle = i\hbar \frac{\partial}{\partial t} |\psi(t)\rangle, \quad (2)$$

and the full description of the Hamiltonian \hat{H} is given in [1,2]. The coordinate-space part of the Hamiltonian \hat{H} is easily diagonalizable in the mode Hilbert space, making it mathematically homomorphic (analogous) to harmonic oscillators uncoupled from each other. This is the popular approach in quantum optics (QO). Then, using this QO approach, we characterize how photons, transported in the form of electromagnetic (EM) fields, interfere with each other. Together with quantum theory, QO has spurred the development of various quantum technologies [6–11] in which few-photon interference and their granularity are important for their quantum effects.

Nevertheless, early pioneers have mathematically shown that one can employ the *macroscopic* framework on quantum electrodynamics (QED) which admits the partial use of the macroscopic Maxwell's theory. This theory uses the concept of effective EM media [5,12,13] when the optical and microwave photon wavelengths are typically much larger than the size of the atoms or molecules. Moreover, it is important to find the normal modes in the form of traveling waves for canonical quantization in these media [12,14,15].

More recently, quantization procedures in general dispersive, dissipative, anisotropic, or reciprocal media [1,2,5,16–21] were developed. A variety of quantum-optical phenomena can be captured by macroscopic QED theory, such as spontaneous emissions rates [22–24] in dielectric media [17], Casimir forces [25], artificial atoms [26], few-photon interference in passive and lossless quantum-optical instruments [27], quantum-optical metamaterials [28], NOON states in quantum metrology, and quantum sensing [29,30], just to name a few.

In this work, we propose a *numerical canonical quantization methodology*, which is useful for numerical experiments on arbitrary passive and lossless quantum-optical systems for

*wccchew@purdue.edu

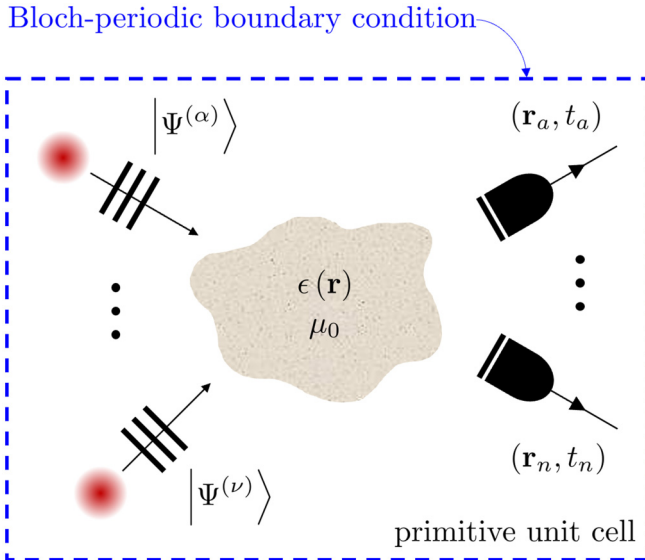


FIG. 1. Two-dimensional illustration of arbitrary passive and lossless quantum-optical systems driven by multiple photons. The systems can be modeled by inhomogeneous dielectric media. The Bloch-periodic boundary condition can be used to extract traveling-wave normal modes and retain the Hermiticity of quantum Maxwell's equations.

nondispersive media [31], as illustrated in Fig. 1. This is valid over the bandwidth where the frequency dispersive effect can be ignored. Based on the macroscopic QED theory, such systems can be modeled by linear, reciprocal, isotropic, nondispersive, and inhomogeneous dielectric media. But here, instead of *ad hoc* analytic normal modes [4,10,32–39], we construct complete and time-reversible numerical normal modes in the form of traveling waves to diagonalize the coordinate-space part of the Hamiltonian. In other words, borrowing the concept of computational electromagnetics (CEM), we directly solve the Helmholtz wave equations for the media by using either the finite-element or finite-difference method on a given mesh.

The present methodology provides a pathway to use new macroscopic QED theory to mathematically model quantum-optical systems with little physical restrictions in a real experimental setup. Eventually, as has happened in the classical electromagnetic case, it would provide a numerical experimental platform to explore a large variety of perplexing QED and quantum-optical phenomena such as virtual photons, quantum-optical metamaterials, superluminal photons by quantum tunneling, interaction-free measurement, quantum metrology and quantum sensing, and time entanglement [40]. This is increasingly important as quantum technologies become increasingly complex.

The numerical canonical quantization here resembles the analytical canonical quantization. The difference is that the modes are found numerically and then quantized analytically. Then quantum information can be injected into these modes, displaying their quantum effects. The modes are formed into wave packets, and we liken the photons to be “riding” on the wave packet formed by these modes.

Beyond canonical quantization in free space, real-world QEM-QO problems typically involve medium inhomogeneity, anisotropy, dispersion, and loss. Our current work tackles the problems related to the medium inhomogeneity and multiphoton interference for which the modal approach is best suited. To do so, we conduct rigorous EM quantization in inhomogeneous dielectric media based on the principle of uncoupled harmonic oscillators. In future work, we will explore the incorporation of anisotropy, dispersion, and loss, as has been expounded in the literature [1,2,12,14,16,17,19–21,41–49], as well as the use of finite-difference time-domain methods to solve these quantum Maxwell's equations [50]. We will also explore the use of Green's function methods [19,44,45,51,52]. The Green's function method has been used to study quantum effects in the spontaneous emission rate [22,23] and Casimir forces in arbitrary geometries [53–56]. Via the developed algorithm, we perform quantum numerical simulations of two-photon interference occurring in a 50:50 beam splitter to observe the Hong-Ou-Mandel effect [57,58].

It should be noted that the quantum Maxwell's equations are Hermitian. To retain the Hermiticity of these equations, we solve these equations with the Bloch-periodic boundary conditions using either the finite-difference (FDM) or finite-element method (FEM).

It should be emphasized that this paper is not on developing advanced CEM algorithms but provides a guideline to incorporate QEM-QO effects into complex solutions of quantum Maxwell's equations by utilizing conventional CEM tools. Any existing commercial EM software does not have a module or package that fully integrates classical and quantum aspects of EM fields. The QED module that we are imagining gets input parameters set by users and ultimately reproduces results typically observed in quantum-optics experiments. For example, for quantum scattering problems, important for quantum biosensing and imaging technologies, users can set up the dielectric property and geometry of media and carrier frequency and bandwidths. Or users can set up entangled photons such that the QEM module can simulate coincidence counts. They can also evaluate higher-order correlations between different photon detectors or the time evolution of the expectation value of the local energy density of photons. Beyond the present work, we are currently developing advanced algorithms that can account for dispersion and dissipation effects by media based on the Green's function approach as well as quantum finite-difference time-domain methods. Furthermore, the incorporation of field-atom interactions into these algorithms would allow one to perform various kinds of virtual quantum-optics experiments to help with the maturing of quantum technologies. To do so, one should rigorously solve both the coordinate part of the quantum Maxwell's equations (1) and quantum state equation (2). Nevertheless, to extract numerical normal modes, one may utilize eigensolvers provided by COMSOL, HFSS, FEKO, or CST MICROWAVE STUDIO. But to incorporate the solutions to the quantum state equation (2), one would have to write additional algorithms, as expounded by this work.

Note that the time convention $e^{-i\omega t}$ is suppressed throughout this work.

II. CANONICAL QUANTIZATION FOR INHOMOGENEOUS DIELECTRIC MEDIA

Consider a three-dimensional (3D) periodic vacuum box, sized by V (m^3), including an arbitrary inhomogeneous dielectric medium (nondispersive and lossless), as illustrated in Fig. 1. Then, the corresponding permittivity is a periodic function as

$$\epsilon(\mathbf{r}) = \epsilon(\mathbf{r} + \mathbf{R}), \quad (3)$$

where \mathbf{R} is a primitive lattice translation vector. In the modal approach, the resulting vector potential operator can be expanded by a countably infinite and complete set of normal modes [1,2,12,14] as

$$\hat{\mathbf{A}}(\mathbf{r}, t) = \hat{\mathbf{A}}^{(+)}(\mathbf{r}, t) + \hat{\mathbf{A}}^{(-)}(\mathbf{r}, t), \quad (4)$$

where its positive and negative frequency components [59] are

$$\hat{\mathbf{A}}^{(+)}(\mathbf{r}, t) = \sum_p \sqrt{\frac{\hbar}{2\omega_{\kappa_p}}} \mathbf{A}_{\kappa_p}(\mathbf{r}) \hat{a}_{\kappa_p}(t), \quad (5)$$

$$\hat{\mathbf{A}}^{(-)}(\mathbf{r}, t) = \sum_p \sqrt{\frac{\hbar}{2\omega_{\kappa_p}}} \mathbf{A}_{\kappa_p}^*(\mathbf{r}) \hat{a}_{\kappa_p}^\dagger(t) \quad (6)$$

and \mathbf{A}_{κ_p} , ω_{κ_p} , \hat{a}_{κ_p} , and $\hat{a}_{\kappa_p}^\dagger$ are the p th normal mode, eigenfrequency, and annihilation and creation operators, respectively. Note that the modal index κ_p implicitly incorporates the vectorial wave number and polarization.

The equal-time commutator relations for ladder operators is given by

$$[\hat{a}_{\kappa_p}(t), \hat{a}_{\kappa_{p'}}^\dagger(t)] = \delta_{\kappa_p, \kappa_{p'}}, \quad (7)$$

$$[\hat{a}_{\kappa_p}(t), \hat{a}_{\kappa_{p'}}(t)] = [\hat{a}_{\kappa_p}^\dagger(t), \hat{a}_{\kappa_{p'}}^\dagger(t)] = 0. \quad (8)$$

Obeying the equations of motion of a classical pendulum expressed in the rotating-wave picture, the ladder operators have the following time dependences:

$$\hat{a}_{\kappa_p}(t) = e^{-i\omega_{\kappa_p}t} \hat{a}_{\kappa_p}, \quad (9)$$

$$\hat{a}_{\kappa_p}^\dagger(t) = e^{i\omega_{\kappa_p}t} \hat{a}_{\kappa_p}^\dagger. \quad (10)$$

The completeness of normal modes yields the orthonormal condition [1,2,60]

$$\int_V d\mathbf{r} [\epsilon(\mathbf{r}) \mathbf{A}_{\kappa_p}^*(\mathbf{r}) \cdot \mathbf{A}_{\kappa_{p'}}(\mathbf{r})] = \delta_{\kappa_p, \kappa_{p'}}. \quad (11)$$

As a result, the corresponding Hamiltonian operator is diagonalized in coordinate space. Then the quantized Hamiltonian in terms of the number operators is

$$\hat{H} = \sum_p \hbar\omega_{\kappa_p} \hat{a}_{\kappa_p}^\dagger \hat{a}_{\kappa_p} = \sum_p \hat{H}_{\kappa_p}, \quad (12)$$

where the zero-point energy is ignored. Thus, eigenstates of number operators are multimode Fock (number) states [38,61,62].

III. CLASSICAL COMPUTATION PART

A. Helmholtz wave equation

For relativistic invariance, classical vector potentials should be associated with scalar potentials through the generalized Lorenz gauge [63]. When external sources are at infinity, by letting $\Phi = 0$, the generalized Lorenz gauge is equivalent to the generalized Coulomb gauge [64]. Then, normal modes are eigenfunctions of the following Helmholtz wave equation:

$$\nabla \times \nabla \times \mathbf{A}_{\kappa_p}(\mathbf{r}) - \omega_{\kappa_p}^2 \epsilon(\mathbf{r}) \mu_0 \mathbf{A}_{\kappa_p}(\mathbf{r}) = 0, \quad (13)$$

with the $\Phi = 0$ gauge, and as a result, (13) can be simplified further as

$$\nabla^2 \mathbf{A}_{\kappa_p}(\mathbf{r}) + \omega_{\kappa_p}^2 \epsilon(\mathbf{r}) \mu_0 \mathbf{A}_{\kappa_p}(\mathbf{r}) = 0. \quad (14)$$

Our prototype model here is available for one dimension (along the x direction) and two dimensions (on the xy plane) with TM_z polarization.

B. Numerical normal modes

To solve (14) for numerical normal modes. We consider a one-dimensional (1D) scalar problem with a mesh (length L , in meters) consisting of a number of nodes $N^{(0)}$, denoted by $\mathbf{r}_i = \hat{x}x_i = \hat{x}(i\Delta x)$ for $i = 1, 2, \dots, N^{(0)}$, where Δx is the grid spacing. We discretize $\mathbf{A}_{\kappa_p}(\mathbf{r}) = \hat{z}\phi_{\kappa_p}(x)$ on nodes of the mesh by applying FEM or FDM with Bloch-periodic boundary conditions (B-PBCs). Then Eq. (14) reduces to a generalized linear eigenvalue problem,

$$\bar{\mathbf{S}} \cdot \bar{\boldsymbol{\phi}} + \bar{\mathbf{M}} \cdot \bar{\boldsymbol{\phi}} \cdot \bar{\boldsymbol{\lambda}} = 0, \quad (15)$$

where $\bar{\mathbf{S}}$ and $\bar{\mathbf{M}}$ are (Hermitian and sparse) stiffness and mass matrices, $\bar{\boldsymbol{\phi}}$ is a matrix including all eigenvectors, and $\bar{\boldsymbol{\lambda}}$ is a diagonal matrix with diagonal eigenvalues. Their elements are given by

$$[\bar{\boldsymbol{\phi}}]_{i,p} = \phi_{\kappa_p}(x_i), \quad (16)$$

$$[\bar{\boldsymbol{\lambda}}]_{p,p} = \mu_0 \omega_{\kappa_p}^2 \quad (17)$$

for $i = 1, 2, \dots, N^{(0)}$ and $p = 1, 2, \dots, N_\kappa = N_0 - 1$. Hence, one can obtain the countably finite numerical normal modes. The numerical modes are normalized to satisfy the orthonormal condition [1,2,65]

$$\bar{\boldsymbol{\phi}}^\dagger \cdot \bar{\mathbf{M}} \cdot \bar{\boldsymbol{\phi}} = (\bar{\boldsymbol{\phi}}^\dagger \cdot \bar{\mathbf{C}}^\dagger) \cdot (\bar{\mathbf{C}} \cdot \bar{\boldsymbol{\phi}}) = \bar{\mathbf{I}}, \quad (18)$$

where $\bar{\mathbf{C}}$ is the Cholesky decomposition of $\bar{\mathbf{M}}$, i.e., $\bar{\mathbf{M}} = \bar{\mathbf{C}}^\dagger \cdot \bar{\mathbf{C}}$, and $\bar{\mathbf{I}}$ is the identity matrix. Note that $\bar{\mathbf{C}} \cdot \bar{\boldsymbol{\phi}}$ is a unitary matrix.

Eventually, the discrete representation of (5) and (6) for the 1D case can be written as

$$\hat{\mathbf{A}}^{(+)}(t) = \bar{\boldsymbol{\phi}} \cdot \bar{\mathbf{D}}(t) \cdot \hat{\mathbf{a}}, \quad (19)$$

$$\hat{\mathbf{A}}^{(-)}(t) = \hat{\mathbf{a}}^\dagger \cdot \bar{\mathbf{D}}^\dagger(t) \cdot \bar{\boldsymbol{\phi}}^\dagger, \quad (20)$$

where

$$[\hat{\mathbf{A}}^{(+)}(t)]_i = \hat{A}^{(+)}(x_i, t), \quad (21)$$

$$[\bar{\mathbf{D}}(t)]_{p,p} = \sqrt{\frac{\hbar}{2\omega_{\kappa_p}}} e^{i\omega_{\kappa_p}t}, \quad (22)$$

$$[\hat{\mathbf{a}}]_p = \hat{a}_{\kappa_p}. \quad (23)$$

In the above, $\bar{\mathbf{D}}$ is a diagonal matrix.

C. Bloch-periodic boundary conditions

In order to retain the Hermiticity of the equations for quantization in the numerical world, we use the Bloch-periodic boundary condition. [Normally, in classical EM simulations, one uses absorbing boundary conditions such as perfectly matched layers or radiation boundary conditions. However, their use gives rise to non-Hermitian equations, and the linear system matrices (stiffness or mass matrices) become non-Hermitian, and the orthogonality and completeness of the system modes cannot be proved.] On the other hand, the use of B-PBCs retains the Hermiticity of the system in (15), implying that eigenfrequencies are always real and normal modes are complete, and energy conserving as well [66].

The spatial length of photon wave packet here is assumed to be much shorter than the size of primitive cell. Note that B-PBCs always return traveling-wave normal modes except for $\theta_0 = 0$ or $\pm\pi$ (edges of passbands) [67]. In addition, we employ a partial solve of (15) to search only the subset of numerical normal modes whose eigenfrequencies are close to the carrier frequencies of photon wave packets. Although the use of B-PBCs requires a proper time windowing to prevent aliases of local dynamics of photon wave packets, we do this in the quest for mathematical rigor and physical clarity. More details can be found in [68].

IV. QUANTUM COMPUTATION PART

A. Initial quantum states for photons

Consider a nonentangled single photon riding on a wave packet [4] that is localized around x_0 with standard deviation σ_0 and center carrier wave number κ_0 . The corresponding initial quantum state can be represented by the linear superposition of multimode Fock states

$$|\Psi^{(1)}\rangle = \sum_{p=1}^{N_\kappa} \tilde{w}_{\kappa_p} |1\rangle_{\kappa_p} = \sum_{p=1}^{N_\kappa} \tilde{w}_{\kappa_p} \hat{a}_{\kappa_p}^\dagger |0\rangle = \hat{\mathbf{a}}^\dagger \cdot \tilde{\mathbf{w}} |0\rangle, \quad (24)$$

where $[\tilde{\mathbf{w}}]_p = \tilde{w}_{\kappa_p}$ is the probability amplitude of $|1\rangle_{\kappa_p}$ that incorporates the spectral amplitude of the wave packet. By the normalization condition, $\tilde{\mathbf{w}}^\dagger \cdot \tilde{\mathbf{w}} = 1$. The above implies that a single photon is “riding” on a localized wave packet traveling through space. The above is the “mode-space” representation of the wave packet, but it also has its corresponding coordinate-space representation [69]. The probability amplitude in mode space can be related to that in coordinate space via the orthonormal relation (18) as

$$\tilde{\mathbf{w}} = (\vec{\phi}^\dagger \cdot \vec{\mathbf{C}}^\dagger) \cdot \mathbf{w}, \quad (25)$$

where $[\mathbf{w}]_i$ is the wave-packet value evaluated at the i th node. For example, in coordinate space, Gaussian and Lorentzian wave packets can be modeled as

$$[\mathbf{w}_{(g)}]_i = w_n e^{-\frac{(x_i - x_0)^2}{2\sigma_0^2}} e^{i\kappa_0(x_i - x_0)}, \quad (26)$$

$$[\mathbf{w}_{(l)}]_i = w_n e^{-\frac{|x_i - x_0|}{\sigma_0}} e^{i\kappa_0(x_i - x_0)}, \quad (27)$$

where w_n is a normalization factor for which $\mathbf{w}^\dagger \cdot \mathbf{w} = 1$. Hence, the photon does not have a definite momentum or energy and becomes momentum or energy uncertain (see [4], Chap. 12).

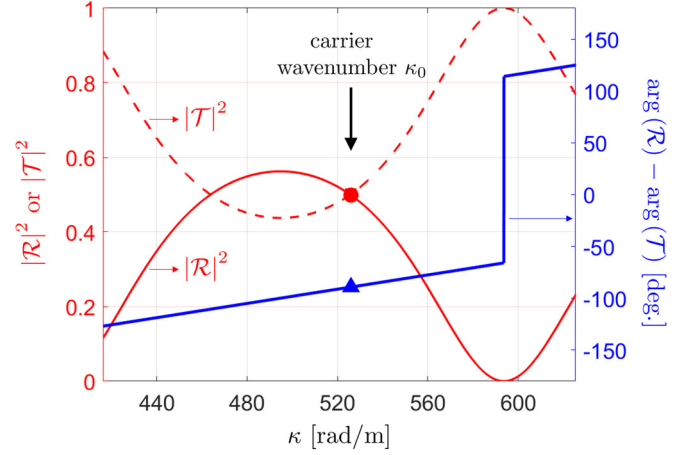


FIG. 2. Reflectivity (red solid line), transmittivity (red dashed line), and relative phase difference (blue solid line) of the designed beam splitter (BS). When $\kappa = \kappa_0 = 526$ rad/m, the BS yields almost equal amplitudes and a 90° relative phase difference in reflected and transmission coefficients.

For two nonentangled photons, the corresponding initial quantum state is given by the tensor product of two individual single-photon quantum states as

$$|\Psi^{(2)}\rangle = |\Psi_B^{(1)}\rangle \otimes |\Psi_A^{(1)}\rangle = (\hat{\mathbf{a}}^\dagger \cdot \tilde{\mathbf{w}}_{(B)}) (\hat{\mathbf{a}}^\dagger \cdot \tilde{\mathbf{w}}_{(A)}) |0\rangle, \quad (28)$$

where $\tilde{\mathbf{w}}_{(A)}$ and $\tilde{\mathbf{w}}_{(B)}$ are probability amplitudes of A and B photons, respectively. Notice that the above remains unchanged when the order of the two terms on the right-hand side is swapped. This implies that these two photons are indistinguishable.

B. Expectation value of arbitrary observables

In the classical regime, the EM apparatus can measure deterministic voltages, currents, or fields. To account for the quantum nature of electromagnetic fields, QEM-QO experiments employ the (spatial or temporal) coincidence count using photodetectors. The second-order correlation function mathematically models the coincidence count. In quantum numerical simulations with few physical restrictions, one can observe various measurable quantities, such as the expectation value of energy density and higher-order correlation functions. For instance, the second-order correlation can be evaluated via (29), and the expectation value of more general observables can be modeled as (31). These quantities are basically involved in the linear superposition of the arbitrary

TABLE I. Parameter setup for the 1D BS simulation where L and L_s are Bloch period and slab thickness, respectively. $N_s^{(0)}$ is the number of sample points in the slab.

Continuum parameters	Discrete parameters		Wave packet information		
	Value	Value	Value	Value	
L	6 m	$N^{(0)}$	16,001	x_0	1.5 m
L_s	6 mm	Δx	0.375 mm	σ_0	1.2 m
ϵ_s	$7\epsilon_0$ F/m	$N_s^{(0)}$	17	κ_0	526 rad/m

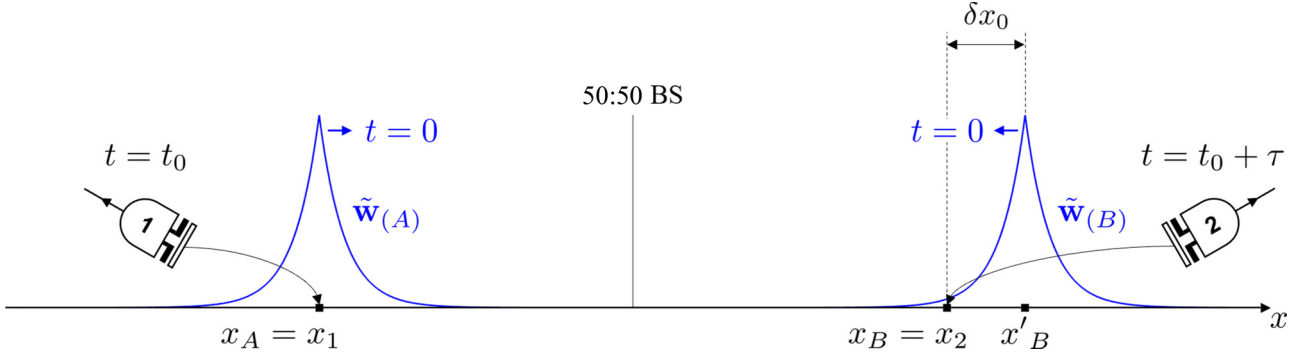


FIG. 3. Schematic of 1D quantum numerical simulations for two-photon incidence in a 50:50 beam splitter (BS). Two spatially localized (nonentangled) photons are sent from different inputs to the BS when $t = 0$ s. After the destructive interference in the BS, we detect photons at both outputs when $t = t_0$ s to evaluate the second-order correlation functions. To observe the Hong-Ou-Mandel effect, we perturb the initial localization position of the photon on the right side by δx_0 .

product of ladder operators acting on multimode Fock states. Here, we develop an algorithm to deal with such pertinent quantum calculations (see the Appendix).

V. QUANTUM NUMERICAL SIMULATIONS

A. Hong-Ou-Mandel effect in a 1D beam splitter

To observe the Hong-Ou-Mandel (HOM) effect [57,58], we use a single dielectric slab for a 50:50 beam splitter (BS) with a 90° relative phase difference. After a parametric study of reflection and transmission [70] at the dielectric slab, we set the relative permittivity of the slab $\epsilon_s = 7\epsilon_0$ F/m and the thickness $L_s = 6$ mm. Figure 2 illustrates $|\mathcal{R}|^2$ and $|\mathcal{T}|^2$ (measured on the vertical left axis) and $\arg(\mathcal{R}) - \arg(\mathcal{T})$ (measured on the vertical right axis) over the operating wave number κ . It should be noted that even though mate-

rial dispersion is ignored, geometrical dispersion is present due to the finite thickness of the beam splitter. When $\kappa = 526$ rad/m, $|\mathcal{R}|^2 \approx 0.4987$, $|\mathcal{T}|^2 \approx 0.5013$, and $\arg(\mathcal{R}) - \arg(\mathcal{T}) \approx -89.16^\circ$; hence, $\kappa_0 = 526$ rad/m will be chosen for a center carrier wave number of photon wave packets for later use. All parameters used in 1D BS simulations are shown in Table I.

Assume that two nonentangled photons are initially localized at $x = x_A = x_1$ and $x = x_B = x_2$, respectively, as illustrated in Fig. 3. The corresponding initial quantum state can be prepared as described in (28). Then, we perturb x_B by δx_0 , viz., $x'_B = x_B + \delta x_0$, to observe the temporal delay effect. After the interference, we place two photodetectors at x_1 and x_2 that detect photons at $t = t_0$ and $t = t_0 + \tau$, respectively. Note that $t_0 = 2x_0/c$ and $\tau = \delta x_0/c$. The second-order correlation function [71,72], denoted by $g^{(2)}$, can be written as

$$g^{(2)}(\tau) = \frac{\langle \Psi^{(2)} | \hat{A}^{(-)}(x_1, t_0) \hat{A}^{(-)}(x_2, t_0 + \tau) \hat{A}^{(+)}(x_2, t_0 + \tau) \hat{A}^{(+)}(x_1, t_0) | \Psi^{(2)} \rangle}{\langle \Psi^{(2)} | \hat{A}^{(-)}(x_1, t_0) \hat{A}^{(+)}(x_1, t_0) | \Psi^{(2)} \rangle \langle \Psi^{(2)} | \hat{A}^{(-)}(x_2, t_0 + \tau) \hat{A}^{(+)}(x_2, t_0 + \tau) | \Psi^{(2)} \rangle} = \frac{\gamma_1}{\gamma_2 \gamma_3}, \quad (29)$$

where τ is a free variable,

$$\gamma_1 = \langle 0 | (\tilde{\mathbf{w}}_{(A)}^\dagger \cdot \hat{\mathbf{a}}) (\tilde{\mathbf{w}}_{(B')}^\dagger \cdot \hat{\mathbf{a}}) (\hat{\mathbf{a}}^\dagger \cdot \boldsymbol{\alpha}_{(1)}^*) (\hat{\mathbf{a}}^\dagger \cdot \boldsymbol{\alpha}_{(2)}^*) (\boldsymbol{\alpha}_{(2)}' \cdot \hat{\mathbf{a}}) (\boldsymbol{\alpha}_{(1)}' \cdot \hat{\mathbf{a}}) (\hat{\mathbf{a}}^\dagger \cdot \tilde{\mathbf{w}}_{(B')}) (\hat{\mathbf{a}}^\dagger \cdot \tilde{\mathbf{w}}_{(A)}) | 0 \rangle,$$

$$\gamma_2 = \langle 0 | (\tilde{\mathbf{w}}_{(A)}^\dagger \cdot \hat{\mathbf{a}}) (\tilde{\mathbf{w}}_{(B')}^\dagger \cdot \hat{\mathbf{a}}) (\hat{\mathbf{a}}^\dagger \cdot \boldsymbol{\alpha}_{(1)}^*) (\boldsymbol{\alpha}_{(1)}' \cdot \hat{\mathbf{a}}) (\hat{\mathbf{a}}^\dagger \cdot \tilde{\mathbf{w}}_{(B)}) (\hat{\mathbf{a}}^\dagger \cdot \tilde{\mathbf{w}}_{(A)}) | 0 \rangle,$$

$$\gamma_3 = \langle 0 | (\tilde{\mathbf{w}}_{(A)}^\dagger \cdot \hat{\mathbf{a}}) (\tilde{\mathbf{w}}_{(B')}^\dagger \cdot \hat{\mathbf{a}}) (\hat{\mathbf{a}}^\dagger \cdot \boldsymbol{\alpha}_{(2)}^*) (\boldsymbol{\alpha}_{(2)}' \cdot \hat{\mathbf{a}}) (\hat{\mathbf{a}}^\dagger \cdot \tilde{\mathbf{w}}_{(B')}) (\hat{\mathbf{a}}^\dagger \cdot \tilde{\mathbf{w}}_{(A)}) | 0 \rangle,$$

$[\boldsymbol{\alpha}_{(1)}]_p = [\tilde{\boldsymbol{\phi}}]_{i_1, p} \cdot [\tilde{\mathbf{D}}(t_0)]_{p, p}$, and $[\boldsymbol{\alpha}_{(2)}]_p = [\tilde{\boldsymbol{\phi}}]_{i_2, p} \cdot [\tilde{\mathbf{D}}(t_0 + \tau)]_{p, p}$. Note that i_1 and i_2 are node indices for which $x_{i_1} = x_1$ and $x_{i_2} = x_2$. One can refer to the Appendix to evaluate (29).

Figure 4 depicts $g^{(2)}(\tau)$ versus τ for Gaussian and Lorentzian wave packets. As expected, when $\tau = 0$, both cases produce HOM dips approaching almost zero since the pair of photons experiences the destructive interference in the BS. We compare our simulation (FEM or FDM) and analytic results. The analytic normal modes for the ideal 50:50 BS

(zero length) are given by

$$\phi_{\kappa_p}(x) = \begin{cases} e^{i\kappa_p x} + \mathcal{R}_0 e^{-i\kappa_p x} & \text{for } \text{sgn}(\kappa_p)x < 0, \\ \mathcal{T}_0 e^{i\kappa_p x} & \text{for } \text{sgn}(\kappa_p)x > 0, \end{cases} \quad (30)$$

where $\mathcal{R}_0 = i/\sqrt{2}$ and $\mathcal{T}_0 = 1/\sqrt{2}$. There is excellent agreement in all three methods for both cases. Furthermore, analytic and numerically evaluated HOM curves are Gaussian and Laplace distributions. This is also in agreement with the theoretical explanation [73]; that is, the power spectrum of wave packets determines the shapes of HOM curves. It should

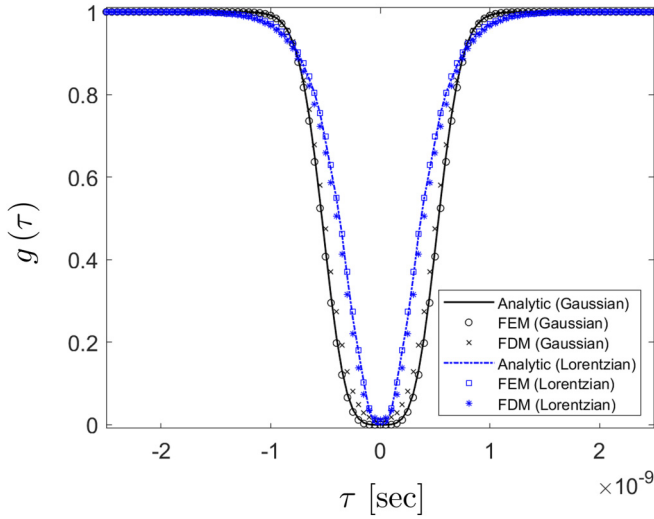


FIG. 4. The Hong-Ou-Mandel (HOM) effects are numerically evaluated for Gaussian (black) and Lorentzian (blue) wave-packet incidences. The resulting HOM curves have Gaussian and Laplace distributions since the power spectrum of wave packets determines the shapes of HOM curves. For each wave-packet incidence, we compare FEM and FDM results, with analytic results showing good agreement among them.

be mentioned that the HOM dip, shown in Fig. 4, is less than one half, which is entirely a quantum effect unachievable by classical Maxwell's theory, which produces a dip that is always greater than one half depending on the type of incident fields such as coherent pulses and chaotic lights [74,75].

Through the developed algorithm, one can easily evaluate higher-order correlation functions for multiphoton interference. Consider an arbitrary (Hermitian) observable \hat{O}_1 as

$$\hat{O}_1 = \prod_{i=1}^{N_o} (\hat{\mathbf{a}}^\dagger \cdot \boldsymbol{\alpha}_{(i)}^*) \prod_{i'=1}^{N_o} (\boldsymbol{\alpha}_{(i')} \cdot \hat{\mathbf{a}}) \quad (31)$$

and an arbitrary initial quantum state for number of nonentangled photons N_p given by

$$|\Psi^{(N_p)}\rangle = \prod_{i=1}^{N_p} (\hat{\mathbf{a}}^\dagger \cdot \tilde{\mathbf{w}}_{(i)}) |0\rangle. \quad (32)$$

Then, the expectation value of \hat{O}_1 becomes

$$\begin{aligned} \langle \Psi^{(N_p)} | \hat{O}_1 | \Psi^{(N_p)} \rangle &= \langle 0 | \prod_{i''=1}^{N_p} (\tilde{\mathbf{w}}_{(i'')}^\dagger \cdot \hat{\mathbf{a}}) \prod_{i''=1}^{N_o} (\hat{\mathbf{a}}^\dagger \cdot \boldsymbol{\alpha}_{(i'')}) \\ &\quad \times \prod_{i'=1}^{N_o} (\boldsymbol{\alpha}_{(i')} \cdot \hat{\mathbf{a}}) \prod_{i=1}^{N_p} (\hat{\mathbf{a}}^\dagger \cdot \tilde{\mathbf{w}}_{(i)}) |0\rangle \\ &= \langle 0 | \hat{O}_2 | 0 \rangle, \end{aligned} \quad (33)$$

which corresponds to the N_o -th-order correlation function. We evaluate the expectation value of \hat{O}_2 with respect to the vacuum state. One can refer to the Appendix for details about its algorithmic implementation.

VI. CONCLUSION

We have shown a computational framework for canonical quantization in arbitrary inhomogeneous dielectric media by incorporating quantum electromagnetics effects into complex solutions of quantum Maxwell's equations. To do so, the proposed algorithm integrated and performed (1) numerical computation of normal modes and (2) evaluation of the linear superposition of arbitrary products of ladder operators acting on multimode Fock states. The former was associated with Hermitian-Helmholtz linear systems solved by the finite-element or finite-difference method; consequently, the complete set of numerical normal modes diagonalizes the Hamiltonian operators to floating-point precision [68]. Based on the developed algorithm, we have performed quantum numerical simulations of two-photon interference occurring in a 50:50 beam splitter to observe the Hong-Ou-Mandel effect. Our prototype model is useful for numerical analyses of various narrow-band quantum-optical multiphoton systems such as quantum metasurfaces, quantum-optical filters, and quantum electrodynamics in open optical cavities.

There are many ways of quantizing electromagnetic fields. The modal approach is simple and appropriate for narrow-band and lossless quantum-optical applications involved in multiphoton interference. And as shown in this work, it rigorously retains the Hermiticity of quantum Maxwell's equations even in the numerical world. It also allows us to solve the quantum state equation (2) easily [68]. In future work, we will also explore various computational electromagnetic methods such as numerical Green's functions and finite-difference or finite-element time-domain methods to develop quantum electromagnetic numerical solvers as shown in [50] and investigate the pros and cons thereof. We will also explore dispersion and dissipation as expounded in [21].

ACKNOWLEDGMENTS

This work is funded by National Science Foundation Grant No. 1818910 and a startup fund at Purdue University. W.C.C. is also funded by Distinguished Visiting Scholars Scheme (DVSS) at the University of Hong Kong (HKU), 2019.

APPENDIX: CALCULATION OF THE DEGREE OF QUANTUM COHERENCE

Here, we provide a specific numerical recipe for calculating arbitrary degrees of quantum coherence that eventually takes the form

$$\langle 0 | \hat{O} | 0 \rangle, \quad (A1)$$

where a Hermitian operator \hat{O} consists of arbitrary products of the weighted sum of annihilation or creation operators. For example, the first-order correlation for a single-photon quantum state vector, which is related to the detection probability of the photon at a specific position and time instant or the expectation value of the energy density, can be

written as

$$\hat{O} = \left(\sum_{p''=1}^{N_k} \beta_{p''}^* \hat{a}_{\kappa_{p''}} \right) \left(\sum_{p'=1}^{N_k} \alpha_{p'}^* \hat{a}_{\kappa_{p'}}^\dagger \right) \left(\sum_{p'=1}^{N_k} \alpha_{p'} \hat{a}_{\kappa_{p'}} \right) \left(\sum_{p=1}^{N_k} \beta_p \hat{a}_{\kappa_p}^\dagger \right), \quad (\text{A2})$$

where α and β are constants associated with the vector potential operator and quantum state vector.

The principles of the present method are based on (1) the *reordering process* and (2) the *constantization process*, which are equivalent to extracting the full contraction terms based on Wick's theorem [76].

1. Reordering process

Consider two operators \hat{A} and \hat{B} which are given by

$$\hat{A} = \sum_{p=1}^{N_k} \alpha_p \hat{a}_{\kappa_p} = (\boldsymbol{\alpha} \cdot \hat{\mathbf{a}}), \quad (\text{A3})$$

$$\hat{B} = \sum_{p=1}^{N_k} \beta_p \hat{a}_{\kappa_p}^\dagger = (\hat{\mathbf{a}}^\dagger \cdot \boldsymbol{\beta}), \quad (\text{A4})$$

where $[\hat{\mathbf{a}}]_p = \hat{a}_{\kappa_p}$, $[\hat{\mathbf{a}}^\dagger]_p = \hat{a}_{\kappa_p}^\dagger$, $[\boldsymbol{\alpha}]_p = \alpha_p$, and $[\boldsymbol{\beta}]_p = \beta_p$. Then, their product $\hat{A}\hat{B}$ is

$$\hat{A}\hat{B} = \left(\sum_{p'=1}^{N_k} \alpha_{p'} \hat{a}_{\kappa_{p'}} \right) \left(\sum_{p=1}^{N_k} \beta_p \hat{a}_{\kappa_p}^\dagger \right) = \sum_{p'=1}^{N_k} \sum_{p=1}^{N_k} \alpha_{p'} \beta_p \hat{a}_{\kappa_{p'}} \hat{a}_{\kappa_p}^\dagger. \quad (\text{A5})$$

By using the commutator relation, (A5) can also be expressed as

$$\begin{aligned} \hat{A}\hat{B} &= \sum_{p'=1}^{N_k} \sum_{p=1}^{N_k} \alpha_{p'} \beta_p (\hat{a}_{\kappa_{p'}}^\dagger \hat{a}_{\kappa_{p'}} + \delta_{p',p} \hat{I}) \\ &= \left(\sum_{p=1}^{N_k} \beta_p \hat{a}_{\kappa_p}^\dagger \right) \left(\sum_{p'=1}^{N_k} \alpha_{p'} \hat{a}_{\kappa_{p'}} \right) + \sum_{p=1}^{N_k} \alpha_p \beta_p \hat{I} \\ &= \hat{B}\hat{A} + \sum_{p=1}^{N_k} \alpha_p \beta_p \hat{I}. \end{aligned} \quad (\text{A6})$$

One can also rewrite (A5) and (A6) in the equivalent matrix representation as

$$\begin{aligned} \hat{A}\hat{B} &= (\boldsymbol{\alpha}' \cdot \hat{\mathbf{a}})(\hat{\mathbf{a}}^\dagger \cdot \boldsymbol{\beta}) \\ &= (\hat{\mathbf{a}}^\dagger \cdot \boldsymbol{\beta})(\boldsymbol{\alpha}' \cdot \hat{\mathbf{a}}) + (\boldsymbol{\alpha}' \cdot \boldsymbol{\beta})\hat{I} \\ &= \hat{B}\hat{A} + (\boldsymbol{\alpha}' \cdot \boldsymbol{\beta})\hat{I}. \end{aligned} \quad (\text{A7})$$

2. Constantization process

Any successive action of a set of creation and annihilation operators to the vacuum state can be replaced by a constant. Consider the product of operators $\hat{A}\hat{B}$ acting on the vacuum; then,

$$\hat{A}\hat{B}|0\rangle = \hat{B}\hat{A}|0\rangle + (\boldsymbol{\alpha}' \cdot \boldsymbol{\beta})\hat{I}|0\rangle = (\boldsymbol{\alpha}' \cdot \boldsymbol{\beta})|0\rangle. \quad (\text{A8})$$

Note that $\hat{B}\hat{A}$ can be thought of as a number operator; hence, $\hat{B}\hat{A}|0\rangle$ always yields zero since the photon occupation number of the ground state is zero, or, mathematically, $\hat{a}_{\kappa_p}|0\rangle = 0$. However, $\hat{A}\hat{B}$ is the Hermitian conjugate of the number operator. Thus, mathematically, the constant $\boldsymbol{\alpha}' \cdot \boldsymbol{\beta}$ should be interpreted as an eigenvalue of $\hat{A}\hat{B}$ with respect to the ground state. In addition, if we take $\langle 0|$ on both sides of (A8), the constant is equal to the vacuum expectation value of $\hat{A}\hat{B}$. For given \hat{A} and \hat{B} , one can award a more specific physical meaning to the constant.

3. First- and second-order correlations for the two-photon quantum state vector

For example, the first-order correlation for two photons is calculated by

$$\begin{aligned} A &= \langle \Psi^{(2)} | \hat{A}^{(-)}(x_i, t) \hat{A}^{(+)}(x_i, t) | \Psi^{(2)} \rangle = \langle 0 | (\boldsymbol{\beta}_1^\dagger \cdot \hat{\mathbf{a}}) \underbrace{(\boldsymbol{\beta}_2^\dagger \cdot \hat{\mathbf{a}})(\hat{\mathbf{a}}^\dagger \cdot \boldsymbol{\alpha}_i^*)}_{\text{use (A7)}} \underbrace{(\boldsymbol{\alpha}'_i \cdot \hat{\mathbf{a}})(\hat{\mathbf{a}}^\dagger \cdot \boldsymbol{\beta}_2)}_{\text{use (A7)}} (\hat{\mathbf{a}}^\dagger \cdot \boldsymbol{\beta}_1) | 0 \rangle \\ &= \langle 0 | (\boldsymbol{\beta}_1^\dagger \cdot \hat{\mathbf{a}}) [(\hat{\mathbf{a}}^\dagger \cdot \boldsymbol{\alpha}_i^*)(\boldsymbol{\beta}_2^\dagger \cdot \hat{\mathbf{a}}) + (\boldsymbol{\beta}_2^\dagger \cdot \boldsymbol{\alpha}_i^*)\hat{I}] [(\hat{\mathbf{a}}^\dagger \cdot \boldsymbol{\beta}_2)(\boldsymbol{\alpha}'_i \cdot \hat{\mathbf{a}}) + (\boldsymbol{\alpha}'_i \cdot \boldsymbol{\beta}_2)\hat{I}] (\hat{\mathbf{a}}^\dagger \cdot \boldsymbol{\beta}_1) | 0 \rangle \\ &= (\boldsymbol{\beta}_2^\dagger \cdot \boldsymbol{\alpha}_i^*)(\boldsymbol{\alpha}'_i \cdot \boldsymbol{\beta}_2) \langle 0 | (\boldsymbol{\beta}_1^\dagger \cdot \hat{\mathbf{a}})(\hat{\mathbf{a}}^\dagger \cdot \boldsymbol{\beta}_1) | 0 \rangle + (\boldsymbol{\beta}_2^\dagger \cdot \boldsymbol{\alpha}_i^*) \langle 0 | (\boldsymbol{\beta}_1^\dagger \cdot \hat{\mathbf{a}})(\hat{\mathbf{a}}^\dagger \cdot \boldsymbol{\beta}_2)(\boldsymbol{\alpha}'_i \cdot \hat{\mathbf{a}})(\hat{\mathbf{a}}^\dagger \cdot \boldsymbol{\beta}_1) | 0 \rangle \\ &\quad + (\boldsymbol{\alpha}'_i \cdot \boldsymbol{\beta}_2) \langle 0 | (\boldsymbol{\beta}_1^\dagger \cdot \hat{\mathbf{a}})(\hat{\mathbf{a}}^\dagger \cdot \boldsymbol{\alpha}_i^*)(\boldsymbol{\beta}_2^\dagger \cdot \hat{\mathbf{a}})(\hat{\mathbf{a}}^\dagger \cdot \boldsymbol{\beta}_1) | 0 \rangle + \langle 0 | (\boldsymbol{\beta}_1^\dagger \cdot \hat{\mathbf{a}})(\hat{\mathbf{a}}^\dagger \cdot \boldsymbol{\alpha}_i^*)(\boldsymbol{\beta}_2^\dagger \cdot \hat{\mathbf{a}})(\hat{\mathbf{a}}^\dagger \cdot \boldsymbol{\beta}_2)(\boldsymbol{\alpha}'_i \cdot \hat{\mathbf{a}})(\hat{\mathbf{a}}^\dagger \cdot \boldsymbol{\beta}_1) | 0 \rangle \\ &\stackrel{\text{use (A8)}}{=} (\boldsymbol{\beta}_2^\dagger \cdot \boldsymbol{\alpha}_i^*)(\boldsymbol{\alpha}'_i \cdot \boldsymbol{\beta}_2)(\boldsymbol{\beta}_1^\dagger \cdot \boldsymbol{\beta}_1) \langle 0 | 0 \rangle + (\boldsymbol{\beta}_2^\dagger \cdot \boldsymbol{\alpha}_i^*)(\boldsymbol{\beta}_1^\dagger \cdot \boldsymbol{\beta}_2)(\boldsymbol{\alpha}'_i \cdot \boldsymbol{\beta}_1) \langle 0 | 0 \rangle + (\boldsymbol{\alpha}'_i \cdot \boldsymbol{\beta}_2)(\boldsymbol{\beta}_1^\dagger \cdot \boldsymbol{\alpha}_i^*)(\boldsymbol{\beta}_2^\dagger \cdot \boldsymbol{\beta}_1) \langle 0 | 0 \rangle \\ &\quad + (\boldsymbol{\beta}_1^\dagger \cdot \boldsymbol{\alpha}_i^*)(\boldsymbol{\beta}_2^\dagger \cdot \boldsymbol{\beta}_2)(\boldsymbol{\alpha}'_i \cdot \boldsymbol{\beta}_1) \langle 0 | 0 \rangle. \end{aligned} \quad (\text{A9})$$

Due to the normalization condition, $\beta_1^\dagger \cdot \beta_1 = \beta_2^\dagger \cdot \beta_2 = 1$. Furthermore, assuming that photons do not share their spectrum, $\beta_2^\dagger \cdot \beta_1 = \beta_1^\dagger \cdot \beta_2 = 0$. Since $\langle 0|0\rangle = 1$ by the orthogonal property of Fock states, one can finally obtain

$$A = (\beta_2^\dagger \cdot \alpha_i^*)(\alpha_i^\dagger \cdot \beta_2) + (\beta_1^\dagger \cdot \alpha_i^*)(\alpha_i^\dagger \cdot \beta_1), \quad (\text{A10})$$

which is proportional to the expectation value of the energy density of EM fields carried by two photons. Note that the inner product $\alpha^t \cdot \beta$ ($\beta^\dagger \cdot \alpha^*$), which is the linear superposition of normal mode values and their weighting factors, describes the positive (negative) frequency component of the resulting EM field values. The above algebra simplifies because of the second-stage diagonalization: The photon-number state, in this case, the vacuum state, is the eigenstate of the photon-number operators. It should be mentioned that the present numerical approach does not deal with quantum states numerically but still uses multimode Fock states for which analytic solutions are available. This is again because of the high quality of the orthonormal property of numerical normal modes (see Fig. 10 in [68]), which permits the second-stage diagonalization of the Hamiltonian operator.

An expectation value of an operator with respect to an arbitrary quantum state, which is basically a scalar value, is of the primary interest in quantum physics. To this end, as shown in (A9), one ends up evaluating the bracket operation of Fock states multiplied by scalar factors. We utilize the orthogonal property of multimode Fock states that converts the bracket

operation into a scalar number. As such, the expectation finally becomes a scalar number, for example, the numerator and denominator of $g^{(2)}$ as in (A10) and (A12).

And the second-order correlation for two photons is $B = \langle B'|B'\rangle$, where

$$\begin{aligned} |B'\rangle &= \hat{A}^{(+)}(x_j, t)\hat{A}^{(+)}(x_i, t)|\Psi^{(2)}\rangle \\ &= (\alpha_j^t \cdot \hat{\mathbf{a}}) \underbrace{(\alpha_i^\dagger \cdot \hat{\mathbf{a}})(\hat{\mathbf{a}}^\dagger \cdot \beta_2)(\hat{\mathbf{a}}^\dagger \cdot \beta_1)}_{\text{use (A7)}}|0\rangle \\ &= (\alpha_j^t \cdot \hat{\mathbf{a}})[(\hat{\mathbf{a}}^\dagger \cdot \beta_2)(\alpha_i^\dagger \cdot \hat{\mathbf{a}}) + (\alpha_i^\dagger \cdot \beta_2)\hat{I}](\hat{\mathbf{a}}^\dagger \cdot \beta_1)|0\rangle \\ &\stackrel{\text{use (A8)}}{=} [(\alpha_j^t \cdot \beta_2)(\alpha_i^\dagger \cdot \beta_1) + (\alpha_i^\dagger \cdot \beta_2)(\alpha_j^t \cdot \beta_1)]|0\rangle. \end{aligned} \quad (\text{A11})$$

In a fashion similar to (A9), one can derive

$$\begin{aligned} B &= [(\alpha_j^t \cdot \beta_2)(\alpha_i^\dagger \cdot \beta_1) + (\alpha_i^\dagger \cdot \beta_2)(\alpha_j^t \cdot \beta_1)]^* \\ &\quad \times [(\alpha_j^t \cdot \beta_2)(\alpha_i^\dagger \cdot \beta_1) + (\alpha_i^\dagger \cdot \beta_2)(\alpha_j^t \cdot \beta_1)], \end{aligned} \quad (\text{A12})$$

which is a scalar value. The above result describes two possible indistinguishable interferences or paths for two photons to experience in a 50:50 quantum beam splitter with a quadrature phase shift. Only when two photons exit through either output while being bunched are probability amplitudes nonzero; otherwise, they are zero.

-
- [1] W. C. Chew, A. Y. Liu, C. Salazar-Lazaro, and W. E. I. Sha, Quantum electromagnetics: A new look-Part I, *J. Multiscale Multiphys. Comput. Tech.* **1**, 73 (2016).
- [2] W. C. Chew, A. Y. Liu, C. Salazar-Lazaro, and W. E. I. Sha, Quantum electromagnetics: A new look-Part II, *J. Multiscale Multiphys. Comput. Tech.* **1**, 85 (2016).
- [3] C. Cohen-Tannoudji, J. Dupont-Roc, and G. Grynberg, *Atom-Photon Interactions: Basic Processes and Applications* (Wiley-VCH, New York, 1988).
- [4] L. Mandel and E. Wolf, *Optical Coherence and Quantum Optics* (Cambridge University Press, Cambridge, 1995).
- [5] S. Scheel and S. Y. Buhmann, Macroscopic quantum electrodynamics, *Acta Phys. Slovaca* **58**, 675 (2008).
- [6] M. A. Nielsen and I. L. Chuang, *Quantum Computation and Quantum Information*, 10th anniversary ed. (Cambridge University Press, Cambridge, 2011).
- [7] N. Gisin, G. Ribordy, W. Tittel, and H. Zbinden, Quantum cryptography, *Rev. Mod. Phys.* **74**, 145 (2002).
- [8] M. Lanzagorta, Quantum radar, *Synth. Lect. Quantum Comput.* **3**, 1 (2011).
- [9] Y. Shih, Quantum imaging, *IEEE J. Sel. Top. Quantum Electron.* **13**, 1016 (2007).
- [10] W. Vogel and D.-G. Welsch, *Quantum Optics* (Wiley, Hoboken, NJ, 2006).
- [11] M. Fox, *Quantum Optics: An Introduction* (Oxford University Press, New York, 2006).
- [12] R. J. Glauber and M. Lewenstein, Quantum optics of dielectric media, *Phys. Rev. A* **43**, 467 (1991).
- [13] J. M. Jauch and K. M. Watson, Phenomenological quantum-electrodynamics, *Phys. Rev.* **74**, 950 (1948).
- [14] L. Knöll, W. Vogel, and D. G. Welsch, Action of passive, lossless optical systems in quantum optics, *Phys. Rev. A* **36**, 3803 (1987).
- [15] In particular, Bloch-Floquet normal modes were used for canonical quantization in periodic structures for the study of characterizing spontaneous emission properties in photonic crystals [77]. But our interest in using Bloch-Floquet modes is quite different, viz., to convert a problem that has infinite number of modes into one with a finite number of modes.
- [16] B. J. Dalton, E. S. Guerra, and P. L. Knight, Field quantization in dielectric media and the generalized multipolar Hamiltonian, *Phys. Rev. A* **54**, 2292 (1996).
- [17] M. E. Crenshaw, Comparison of quantum and classical local-field effects on two-level atoms in a dielectric, *Phys. Rev. A* **78**, 053827 (2008).
- [18] S. L. Adler, Quantum theory of the dielectric constant in real solids, *Phys. Rev.* **126**, 413 (1962).
- [19] H. T. Dung, L. Knöll, and D.-G. Welsch, Three-dimensional quantization of the electromagnetic field in dispersive and absorbing inhomogeneous dielectrics, *Phys. Rev. A* **57**, 3931 (1998).
- [20] T. G. Philbin, Canonical quantization of macroscopic electromagnetism, *New J. Phys.* **12**, 123008 (2010).
- [21] W. E. I. Sha, A. Y. Liu, and W. C. Chew, Dissipative quantum electromagnetics, *J. Multiscale Multiphys. Comput. Tech.* **3**, 198 (2018).
- [22] S. Scheel, L. Knöll, and D.-G. Welsch, Spontaneous decay of an excited atom in an absorbing dielectric, *Phys. Rev. A* **60**, 4094 (1999).

- [23] H. T. Dung, L. Knöll, and D.-G. Welsch, Spontaneous decay in the presence of dispersing and absorbing bodies: General theory and application to a spherical cavity, *Phys. Rev. A* **62**, 053804 (2000).
- [24] P.-F. Qiao, W. E. I. Sha, W. C. H. Choy, and W. C. Chew, Systematic study of spontaneous emission in a two-dimensional arbitrary inhomogeneous environment, *Phys. Rev. A* **83**, 043824 (2011).
- [25] T. G. Philbin, Casimir effect from macroscopic quantum electrodynamics, *New J. Phys.* **13**, 063026 (2011).
- [26] R. Bratschitsch and A. Leitenstorfer, Artificial atoms for quantum optics, *Nat. Mater.* **5**, 855 (2006).
- [27] R. Dumke, Z. Lu, J. Close, N. Robins, A. Weis, M. Mukherjee, G. Birkel, C. Hufnagel, L. Amico, M. G. Boshier, K. Dieckmann, W. Li, and T. C. Killian, Roadmap on quantum optical systems, *J. Opt.* **18**, 093001 (2016).
- [28] P. Georgi, M. Massaro, K.-H. Luo, B. Sain, N. Montaut, H. Herrmann, T. Weiss, G. Li, C. Silberhorn, and T. Zentgraf, Metasurface interferometry toward quantum sensors, *Light: Sci. Appl.* **8**, 70 (2019).
- [29] W. Zhang, M.-X. Dong, D.-S. Ding, S. Shi, K. Wang, Z.-Y. Zhou, G.-C. Guo, and B.-S. Shi, Interfacing a two-photon noon state with an atomic quantum memory, *Phys. Rev. A* **98**, 063820 (2018).
- [30] I. Afek, O. Ambar, and Y. Silberberg, High-NOON states by mixing quantum and classical light, *Science* **328**, 879 (2010).
- [31] Dispersive and lossy media in the manner of [21] will be dealt with in future work.
- [32] M. O. Scully and M. S. Zubairy, *Quantum Optics* (American Association of Physics Teachers, College Park, MD, 1999).
- [33] R. Loudon, *The Quantum Theory of Light* (Oxford University Press, Oxford, 2000).
- [34] C. Gerry and P. Knight, *Introductory Quantum Optics* (Cambridge University Press, Cambridge, 2004).
- [35] D. F. Walls and G. J. Milburn, *Quantum Optics* (Springer, Berlin, 2007).
- [36] J. Garrison and R. Chiao, *Quantum Optics* (Oxford University Press, Oxford, 2008).
- [37] G. Grynberg, A. Aspect, C. Fabre, and C. Cohen-Tannoudji, *Introduction to Quantum Optics: From the Semi-classical Approach to Quantized Light* (Cambridge University Press, Cambridge, 2010).
- [38] W. C. Chew, *Quantum Mechanics Made Simple: Lecture Notes* (CreateSpace Independent Publishing Platform, Scotts Valley, CA, 2015).
- [39] P. Milonni, *An Introduction to Quantum Optics and Quantum Fluctuations* (Oxford University Press, Oxford, 2019).
- [40] C. C. Gerry and K. M. Bruno, *The Quantum Divide: Why Schrödinger's Cat Is Either Dead or Alive* (Oxford University Press, Oxford, 2013).
- [41] P. D. Drummond, Electromagnetic quantization in dispersive inhomogeneous nonlinear dielectrics, *Phys. Rev. A* **42**, 6845 (1990).
- [42] B. Huttner and S. M. Barnett, Quantization of the electromagnetic field in dielectrics, *Phys. Rev. A* **46**, 4306 (1992).
- [43] T. Gruner and D.-G. Welsch, Correlation of radiation-field ground-state fluctuations in a dispersive and lossy dielectric, *Phys. Rev. A* **51**, 3246 (1995).
- [44] T. Gruner and D.-G. Welsch, Quantum-optical input-output relations for dispersive and lossy multilayer dielectric plates, *Phys. Rev. A* **54**, 1661 (1996).
- [45] S. Scheel, L. Knöll, and D.-G. Welsch, QED commutation relations for inhomogeneous Kramers-Kronig dielectrics, *Phys. Rev. A* **58**, 700 (1998).
- [46] A. Tip, Linear absorptive dielectrics, *Phys. Rev. A* **57**, 4818 (1998).
- [47] R. Matloob, Electromagnetic field quantization in an absorbing medium, *Phys. Rev. A* **60**, 50 (1999).
- [48] A. Tip, L. Knöll, S. Scheel, and D.-G. Welsch, Equivalence of the Langevin and auxiliary-field quantization methods for absorbing dielectrics, *Phys. Rev. A* **63**, 043806 (2001).
- [49] L. G. Suttrop and M. Wubs, Field quantization in inhomogeneous absorptive dielectrics, *Phys. Rev. A* **70**, 013816 (2004).
- [50] D.-Y. Na and W. C. Chew, Quantum electromagnetic finite-difference time-domain solver, *Quantum Rep.* **2**, 253 (2020).
- [51] T. Gruner and D.-G. Welsch, Green-function approach to the radiation-field quantization for homogeneous and inhomogeneous Kramers-Kronig dielectrics, *Phys. Rev. A* **53**, 1818 (1996).
- [52] F. S. S. Rosa, D. A. R. Dalvit, and P. W. Milonni, Electromagnetic energy, absorption, and Casimir forces. II. Inhomogeneous dielectric media, *Phys. Rev. A* **84**, 053813 (2011).
- [53] M. S. Tomaš, Casimir force in absorbing multilayers, *Phys. Rev. A* **66**, 052103 (2002).
- [54] A. W. Rodriguez, A. P. McCauley, J. D. Joannopoulos, and S. G. Johnson, Casimir forces in the time domain: Theory, *Phys. Rev. A* **80**, 012115 (2009).
- [55] A. P. McCauley, A. W. Rodriguez, J. D. Joannopoulos, and S. G. Johnson, Casimir forces in the time domain: Applications, *Phys. Rev. A* **81**, 012119 (2010).
- [56] T. Xia, P. R. Atkins, W. E. Sha, and W. C. Chew, Casimir force modeling: Vacuum fluctuation, zero-point energy, and computational electromagnetics, *IEEE Antennas Propag. Mag.* (to be published).
- [57] C. K. Hong, Z. Y. Ou, and L. Mandel, Measurement of Subpicosecond Time Intervals between Two Photons by Interference, *Phys. Rev. Lett.* **59**, 2044 (1987).
- [58] S. Prasad, M. O. Scully, and W. Martienssen, A quantum description of the beam splitter, *Opt. Commun.* **62**, 139 (1987).
- [59] S. L. Hahn, *Hilbert Transforms in Signal Processing* (Artech House, Boston, 1996), Vol. 2.
- [60] W. C. Chew, Lecture notes on theory of guided waves (unpublished).
- [61] D. A. Miller, *Quantum Mechanics for Scientists and Engineers* (Cambridge University Press, Cambridge, 2008).
- [62] K. Gottfried and T.-M. Yan, *Quantum Mechanics: Fundamentals* (CRC Press, Boca Raton, FL, 2018).
- [63] W. C. Chew, Vector potential electromagnetics with generalized gauge for inhomogeneous media: Formulation, *Prog. Electromagn. Res.* **149**, 69 (2014).
- [64] Q. S. Liu, S. Sun, and W. C. Chew, A potential-based integral equation method for low-frequency electromagnetic problems, *IEEE Trans. Antennas Propag.* **66**, 1413 (2018).
- [65] W. C. Chew, *Waves and Fields in Inhomogeneous Media* (IEEE Press, New York, 1996).
- [66] W. Chew, A. Liu, C. Salazar-Lazaro, D.-Y. Na, and W. Sha, Hamilton equations, commutator, and energy conservation, *Quantum Rep.* **1**, 295 (2019).

- [67] J. D. Joannopoulos, S. G. Johnson, J. N. Winn, and R. D. Meade, *Photonic Crystals: Molding the Flow of Light*, 2nd ed. (Princeton University Press, Princeton, NJ, 2008).
- [68] D.-Y. Na, J. Zhu, F. L. Teixeira, and W. C. Chew, Quantum information propagation preserving computational electromagnetics, [arXiv:1911.00947](https://arxiv.org/abs/1911.00947).
- [69] In free space, the mode space would be the Fourier space representation.
- [70] C. Balanis, *Advanced Engineering Electromagnetics* (Wiley, Hoboken, NJ, 2012).
- [71] R. Hanbury-Brown and R. Q. Twiss, Interferometry of the intensity fluctuations in light - I. Basic theory: The correlation between photons in coherent beams of radiation, *Proc. R. Soc. London, Ser. A* **242**, 300 (1957).
- [72] R. J. Glauber, The quantum theory of optical coherence, *Phys. Rev.* **130**, 2529 (1963).
- [73] P. P. Rohde, T. C. Ralph, and M. A. Nielsen, Optimal photons for quantum-information processing, *Phys. Rev. A* **72**, 052332 (2005).
- [74] M. Facão, A. Lopes, A. L. Silva, and P. Silva, Computer simulation for calculating the second-order correlation function of classical and quantum light, *Eur. J. Phys.* **32**, 925 (2011).
- [75] Y.-S. Kim, O. Slattery, P. S. Kuo, and X. Tang, Conditions for two-photon interference with coherent pulses, *Phys. Rev. A* **87**, 063843 (2013).
- [76] G. C. Wick, The evaluation of the collision matrix, *Phys. Rev.* **80**, 268 (1950).
- [77] G. Kweon and N. Lawandy, Quantum electrodynamics in photonic crystals, *Opt. Commun.* **118**, 388 (1995).